

# Polyetherimide-Modified Epoxy Networks: Influence of Cure Conditions on Morphology and Mechanical Properties

E. GIRARD-REYDET, V. VICARD, J. P. PASCAULT, H. SAUTEREAU

Laboratoire des Matériaux Macromoléculaires, UMR CNRS No. 5627, Institut National des Sciences Appliquées de Lyon, Bât. 403 20, Avenue A. Einstein, 69621 Villeurbanne Cedex, France

Received 19 July 1996; accepted 4 November 1996

**ABSTRACT:** The morphologies and mechanical properties of thermoplastic-modified epoxy networks generated through the reaction-induced phase separation procedure were studied as a function of isothermal cure conditions. The selected model system was diglycidyl ether of bisphenol A cured with 4,4'-methylenebis [3-chloro,2,6-diethylaniline] in the presence of a nonfunctionalized polyetherimide. Appropriate precuring and postcuring schedules were selected. The precure temperature had a strong effect on final morphologies because it affected the viscosity of the system at the cloud point and the extent of the separation process. The morphologies generated are discussed in connection with phase separation mechanisms. The ratio of the height of the loss peaks corresponding to each phase was an appropriate parameter to qualitatively predict the shape of morphology and to determine if the system was phase-inverted or not. The fracture toughness,  $K_{Ic}$  was significantly improved only when bicontinuous or inverted structures were generated, resulting from the plastic drawing of the thermoplastic-rich phase. Before phase inversion,  $K_{Ic}$  was hardly higher than that of the neat matrix due to poor interfacial adhesion. Nevertheless, the thermoplastic-rich particles constitute obstacles to the propagation of the crack and contribute to the toughening of the material, measured through impact resistance measurements. The observation of fracture surfaces revealed the occurrence of microcracking and crack-pinning. Strain recovery experiments showed that particle-induced shear yielding of the matrix was present as well. © 1997 John Wiley & Sons, Inc. *J Appl Polym Sci* **65**: 2433–2445, 1997

**Key words:** phase separation; morphology; epoxy toughened thermosets; thermoplastic

## INTRODUCTION

For 10 years, the use of rigid thermoplastics to toughen highly crosslinked epoxy networks has emerged as an alternative to avoid the classical compromises between toughness and thermal stability associated with the rubber toughening. There are two main procedures to generate a second-phase dispersion in a thermosetting polymer. The first one consists of the dispersion of pre-

formed particles in the starting monomers. Several problems arise from the addition of preformed particles. Their size and composition have to be controlled<sup>1,2</sup> and surface treatments are often needed.<sup>2,3</sup> Moreover, the introduction of particles strongly increases the viscosity of the system, which may be a drawback for processing. Last but not least, the quality of the dispersion must be very good to get toughness improvements. The second procedure involves phase separation during polymerization of an initially homogeneous solution. During the isothermal copolycondensation of an initially miscible thermoplastic–monomers mixture, three transformations are expected to oc-

Correspondence to: H. Sautereau.  
Contract grant sponsor: CMEABG.

cur: (a) phase separation, which results from the increasing molar mass of the epoxy-hardener copolymer; (b) gelation; and (c) vitrification of the thermoset. The main advantage of this procedure is the possibility of generating a variety of morphologies within the final material. Either particulate or bicontinuous structures can be generated, depending on modifier concentration, molar mass, temperature, and reaction rate. However, the control of these morphologies is essential to control subsequent mechanical properties. Nevertheless, most studies in the literature only address the increase in toughness obtained, and little progress has been made in controlling morphology since the pioneering work of Bucknall and Partridge.<sup>4</sup> This weakness has been clearly emphasized by Pearson and Yee<sup>5</sup> as well as the lack of understanding of fracture and toughening mechanisms in these systems. These authors mainly focused on these last points.<sup>5,6</sup> It is evident that every factor affecting the thermodynamic, the polymerization kinetics, and the phase separation process should have an influence on final morphologies,<sup>7</sup> and, hence, on mechanical properties.

Unfortunately, varying one parameter may vary both thermodynamic and kinetic factors, making it difficult to provide a simple explanation of the effect of each separate parameter. That is why one finds in the abundant literature devoted to rubber or thermoplastic toughening trends that only fit the author's own results (i.e., it has been reported that the volume fraction of dispersed phase remains practically constant,<sup>8,9</sup> passes through a maximum,<sup>10</sup> or decreases<sup>11</sup> as temperature increases). In this context, this article describes the effect of cure schedules on morphologies and mechanical properties of polyetherimide-modified diglycidyl ether of bisphenol A/4,4'-methylenebis [3-chloro,2,6-diethylaniline] networks. The selected epoxy system is a model system with controlled reactivity.<sup>12</sup> The influence of the additive on polymerization kinetics and the study of the phase separation process have been previously reported.<sup>13-15</sup> Mechanical properties will be discussed not only in terms of fracture toughness improvement but also in terms of impact strength improvement, behavior during strain recovery experiments, and viscoelastic properties in connection with morphologies.

## EXPERIMENTAL

### Materials

The materials used have been described previously.<sup>12,13</sup> A classical diepoxy prepolymer, di-

glycidyl ether of bisphenol A (DGEBA), with a low polydispersity index ( $\bar{w} = 0.03$ ) was used. The hardener was a diamine 4,4'-methylenebis [3-chloro,2,6-diethylaniline] (MCDEA).

The thermoplastic modifier was an amorphous nonfunctionalized polyetherimide (PEI) Ultem 1000 supplied by the General Electric Company.

The chemical structures and characteristics of all reactants are listed in Table I.

The PEI modified mixtures were prepared in a two-step process: PEI was first dissolved at 140°C in the epoxy prepolymer, the diamine was then added at 90°C. The hardener was used at the stoichiometric ratio epoxy to amino-hydrogen groups equal to 1. After stirring under vacuum, the mixture was poured into a PTFE coated iron mold ( $160 \times 160 \times 7$  mm<sup>3</sup>) and then cured (see below).

For the designation of systems, for example, 10P denotes the system DGEBA-MCDEA with 10 wt % of PEI. The term neat means the epoxy system without thermoplastic.

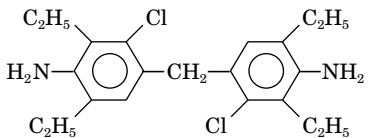
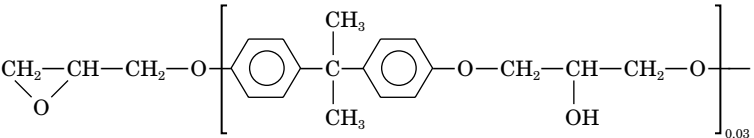
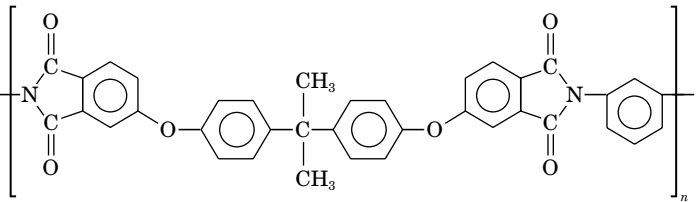
### Techniques

The cloud-point setup was home-made and used visible light and a photo transistor.<sup>9</sup> Dynamical mechanical thermal analysis was performed using a RSA II Rheometrics viscoelasticimeter equipped for rectangular samples in tensile testing. The storage modulus  $E'$  and the loss factor  $\tan \delta$  were measured during temperature sweeps (3°C per step) at a constant frequency 1 Hz and a strain amplitude equal to 0.07%.

The Young's modulus,  $E$ , and Poisson's ratio,  $\nu$ , were obtained from an uniaxial tensile test at room temperature and  $1 \text{ mm} \cdot \text{min}^{-1}$  ( $\dot{\epsilon} = 3 \cdot 10^{-4} \text{ s}^{-1}$ ) on an Adamel Lhomargy (DY25) testing machine using an ISO 60 specimen with bonded Vishay Micromasures crossed strain gages giving both longitudinal and transversal strains.

On the same tensile machine, the uniaxial compression behavior of parallelepiped specimens (section  $6 \times 9 \text{ mm}^2$ , height 12 mm) was investigated (25°C,  $\dot{\epsilon} = 7 \cdot 10^{-4} \text{ s}^{-1}$ ) to determine the upper yield stress,  $\sigma_y$  and to record some evolution of the recovered strain after unloading. We are aware that calculated stresses remain approximative because the stress field is not purely uniaxial. The critical stress intensity factor,  $K_{Ic}$  and the fracture energy,  $G_{Ic}$  were obtained from three-point bending tests performed on single-edge notched specimens (SEN). The procedure proposed by Williams and Cawood<sup>16</sup> was strictly fol-

**Table I** Characteristics of the Different Reactants Used

Reactants	Formula	Supplier	$\overline{M}_n$ (g · mol <sup>-1</sup> )	$\overline{M}_w$ (g · mol <sup>-1</sup> )	$T_g$ (°C)
4,4'-methylenebis[3-chloro 2,6-diethylaniline] (MCDEA)		Lonza	380	/	/
diglycidyl ether of bisphenol A (DGEBA) $\overline{n} = 0.03$		Dow Chemicals DER 332	380	/	-22
polyetherimide (PEI)		General Electric	26,000	50,000	210

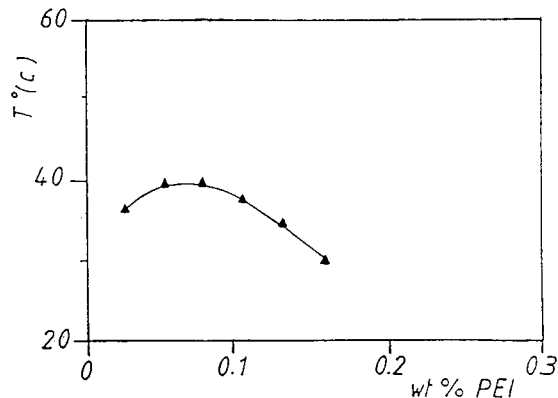


**Figure 1** Initial cloud point curve for the DGEBA-MCDEA/PEI system.

lowed with a crosshead speed of  $10 \text{ mm} \cdot \text{min}^{-1}$ .  $K_{Ic}$  and  $G_{Ic}$  were calculated as the mean values of 10 tests at least.

An instrumented Charpy impact pendulum<sup>17</sup> was used at room temperature and  $3 \text{ m} \cdot \text{s}^{-1}$  with unnotched parallelepiped bars. The surface resilience,  $R_S$  was obtained by dividing the total absorbed energy by the cross-section area (French Standard NF 51035).

The fracture surfaces of broken SEN specimens were examined, after gold sputtering, by scanning electron microscopy (SEM) using a Philips XL20 apparatus (voltage 15 kV).

Morphological micrographs were obtained using a JEM-200CX transmission electron microscope (TEM). Ultrathin sections were prepared at room temperature. A natural contrast existed between phases when a 80 kV accelerating voltage was used. The micrographs were analyzed using a PCI3 image processing software developed in our laboratory. PCI3 can calculate the surface fraction of each phase, the average surface and number per unit area of particles. Assuming isotropic materials for 10P blends, the volume fraction was considered to be the surface fraction.

## RESULTS AND DISCUSSION

### Cure Schedules

The cloud point curve (CPC) of the DGEBA-MCDEA/PEI system before any reaction has taken place is shown in Figure 1. It is typical of systems exhibiting upper critical solution temperature (UCST) behavior. It is worth noting the wide miscibility window available for this system.

The kinetic studies of this modified epoxy sys-

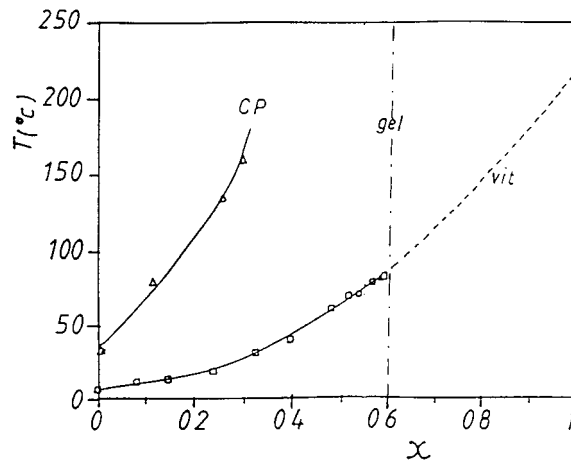


**Figure 2** Experimental phase diagram (temperature vs. epoxy conversion) for the 20P blend: ( $\Delta$ ) cloud points, ( $\square$ ) vitrification, (---) gelation (for the sake of clarity the possible slight evolution of  $x_{\text{gel}}$  with temperature is not considered).

tem were reported elsewhere.<sup>13</sup> For a general discussion, it is important to transform times into conversions. Cloud point conversions were measured for the reactive mixtures, for various PEI amounts, and polycondensation temperatures.<sup>14</sup> All these experimental results could be plotted on a same temperature-conversion-transformation ( $T, x, T$ ) diagram, integrating phase separation ( $T_{cp}, x_{cp}$ ), gelation ( $x_{\text{gel}}$ ) and vitrification ( $T_g, x$ ), as shown in Figure 2 for the 20P blend. Such diagrams are essential to control the curing of blends with appropriate precuring and postcuring schedules. Selected cure schedules are given in Table II. Precure times were chosen larger than vitrification times to be sure that most of the microstructure developed isothermally (for all precure temperatures studied, gelation occurred before vitrification). To obtain the final materials and to ensure a complete network formation without any degradation, all samples were postcured 2 h at  $185^\circ\text{C}$ .

**Table II** Different Cure Schedules Selected

Precure		Postcure	
$T_i$ ( $^\circ\text{C}$ )	$t$ (min)	$T_{PC}$ ( $^\circ\text{C}$ )	$t$ (min)
80	7200	185	120
135	420	185	120
160	240	185	120

## Morphologies

Figure 3(a)–(c) shows the domain structures of 10P systems (10% by weight or 9.2% by volume) observed by TEM, depending on the precure temperature. The bright parts correspond to the epoxy-rich phase ( $\alpha$  phase) and the dark parts correspond to the PEI-rich phase ( $\beta$  phase). The volume fraction of  $\beta$  phase,  $\overline{V}_\beta$ , the average size,  $\overline{S}_\beta$ , and average contour,  $\overline{C}_\beta$  of domains are listed in Table III. It can be first seen that, with 10 wt % of PEI, phase separation produced a dispersed  $\beta$  phase rich in thermoplastic modifier in a continuous  $\alpha$  phase. Considering the shape of  $\beta$  domains, a low precure temperature,  $T_i = 80^\circ\text{C}$ , leads to the formation of some very extensive non-spherical  $\beta$  domains and, the higher the precure temperature, the more spherical the  $\beta$  domains ( $\overline{S}_\beta$  and  $\overline{C}_\beta$  decreases). However, it has been shown<sup>15</sup> that, at this modifier concentration, phase separation proceeded via the spinodal decomposition (SD) mechanism whatever the precure temperature. Due to the very low reactivity of the DGEBA–MCDEA system, SD under non-isoquench conditions was found to be very similar to the classical isoquench SD. Then, in the latest stage of demixing, the initial high degree of phase connectivity is gradually lost due to (a) the minimization of the interfacial area, and (b) the redissolution of  $\beta$  particles insofar as the quench depth keeps on increasing. Nevertheless, the vitrification of the  $\beta$  phase rich in high  $T_g$  thermoplastic affects the level of fragmentation of  $\beta$  domains. The higher  $T_i$  is, the later vitrification of the  $\beta$  phase occurs and the further the phase separation process goes. Therefore, when the precure temperature increases, the extent of phase separation increases ( $\overline{V}_\beta$  decreases) and the extent of fragmentation/coalescence of  $\beta$  domains increases so that spherical particles are obtained for  $T_i = 160^\circ\text{C}$ .

Figure 4(a)–(c) shows the domain structures of 20P systems (20% by weight or 18.6% by volume) observed by TEM. With 20 wt % of PEI, phase separation then leads to the formation of inverted structures ( $T_i = 80^\circ\text{C}$ ) or bicontinuous structures ( $T_i = 135^\circ\text{C}$ ,  $160^\circ\text{C}$ ). This is in good agreement with the theoretical composition of the thermodynamic critical point of the CPC,  $\phi_{\text{MC}} = 10.5$  wt % before any reaction has taken place.<sup>15</sup> Clarke et al.<sup>18</sup> have shown recently that  $\phi_{\text{MC}}$  remained slightly constant upon curing. For this modifier concentration, the precure temperature has a much stronger effect on final morphologies

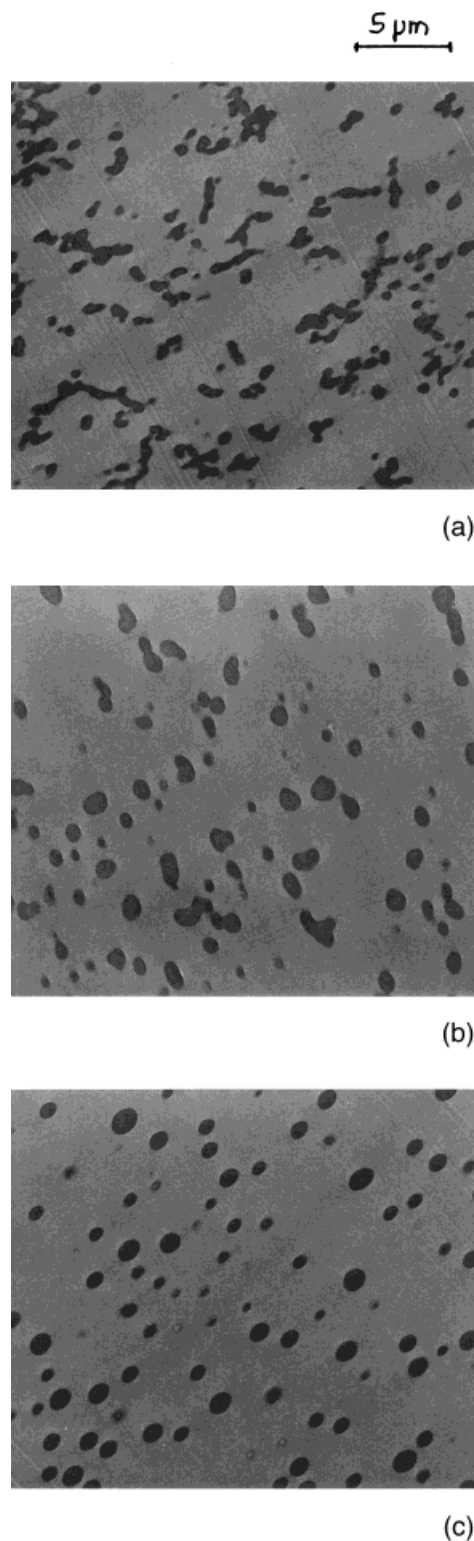


**Figure 3** Transmission electron micrographs of the 10P blends depending on the precure temperature: (a)  $T_i = 80^\circ\text{C}$ , (b)  $T_i = 135^\circ\text{C}$ , (c)  $T_i = 160^\circ\text{C}$ .

**Table III** Volume Fraction of  $\beta$  Phase,  $V_\beta$ , Average Size,  $\overline{S}_\beta$  and Average Contour,  $\overline{C}_\beta$  of  $\beta$  Particles in 10P (9.2% PEI by Volume) Blends Depending on the Precure Temperature,  $T_i$

$T_i$ (°C)	$V_\beta$ (%)	$\overline{S}_\beta$ ( $\mu\text{m}^2$ )	$\overline{C}_\beta$ ( $\mu\text{m}$ )
80	12	0.50	2.7
135	10.5	0.40	2.0
160	10	0.35	1.8

than for 10P blends. In addition to the effect of the vitrification of the  $\beta$  phase, the much higher viscosity of 20P systems could also exacerbate differences in mobility depending on  $T_i$ . Phase separation was found to occur via the SD process as well.<sup>12</sup> In particular, we observed at  $T_i = 80^\circ\text{C}$  first, the development of bicontinuous structures, thereafter, the interruption of the  $\alpha$  phase continuity leading to growing  $\alpha$  domains in a continuous  $\beta$  matrix. One can imagine their growth to go further at higher temperature so that the continuity of the  $\beta$  phase stops as well. It is worth noting the presence of a subinclusions in the  $\beta$  domains for  $T_i = 135^\circ\text{C}$  and especially  $160^\circ\text{C}$ , suggesting secondary phase separation has occurred. These complex morphologies are very close to those reported by Bucknall et al. for an epoxy–diaminodiphenylmethane system modified with 10 wt % of polyethersulfone.<sup>19</sup>

### Dynamic Mechanical Thermal Behavior

Dynamic mechanical data for the neat resin and pure PEI are given in Figure 5. The unmodified resin gives two loss peaks: a low, broad peak with a maximum at  $-68^\circ\text{C}$  assigned to the secondary relaxation of thermoset systems and a main peak corresponding to  $T_g$  at  $184^\circ\text{C}$ . The curve for PEI also exhibits two loss peaks: a much lower and broader secondary peak with a maximum around  $90^\circ\text{C}$ , and a main peak corresponding to  $T_g$  at  $225^\circ\text{C}$ . The principal feature in these curves is the significant temperature difference between the main relaxations of these components. As illustrated Figure 6, the occurrence of phase separation in the blends is characterized by two distinct high-temperature relaxations associated respectively to the  $T_g$  of the epoxy-rich phase ( $\alpha$  phase) and to the  $T_g$  of the PEI-rich phase ( $\beta$  phase). The characteristics of these high-temperature loss peaks, namely the temperatures of maxima ( $T_{m\alpha}$ ,  $T_{m\beta}$ ), their respective heights ( $h_\alpha$ ,  $h_\beta$ ), their width

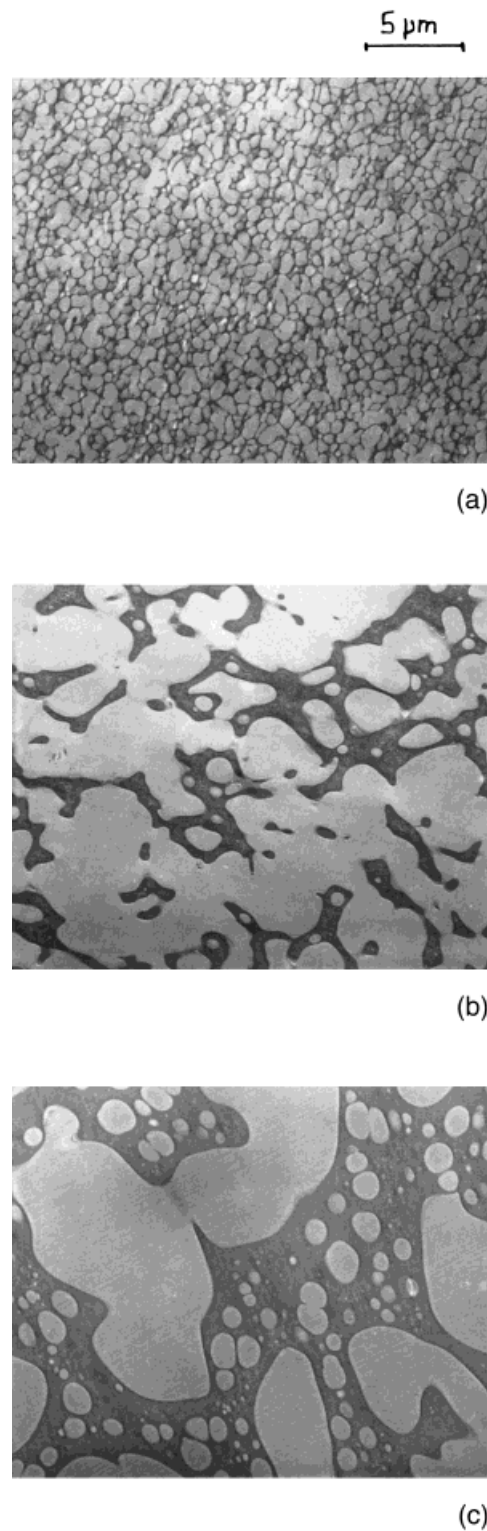


**Figure 4** Transmission electron micrographs of the 20P blends depending on the precure temperature: (a)  $T_i = 80^\circ\text{C}$ , (b)  $T_i = 135^\circ\text{C}$ , (c)  $T_i = 160^\circ\text{C}$ .

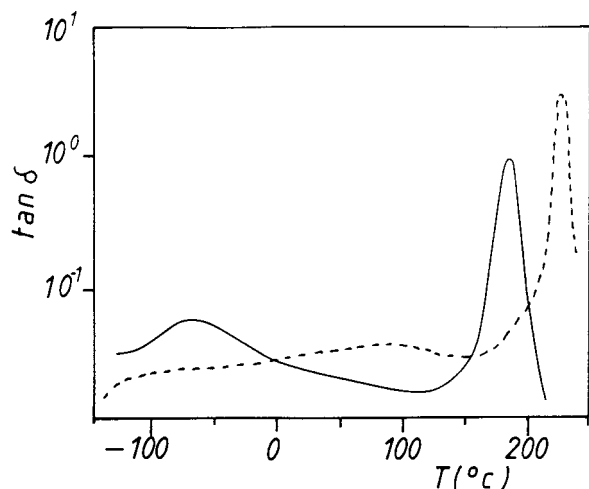


**Figure 5** Dynamic mechanical spectra: loss factor,  $\tan \delta$  vs. temperature for (—) neat epoxy matrix, (-----) pure PEI.

remaining almost constant and the ratio of these heights ( $h_\beta/h_\alpha$ ) are collected in Table IV. The kind of morphology obtained for each system is indicated. First it can be seen that  $T_{m\alpha}$  remains almost constant regardless of modifier concentration and precure temperature. Alternatively,  $T_{m\beta}$  is significantly lower for the pure PEI. This shift can be attributed to the remaining low molar masses epoxy-amine species dissolved in the  $\beta$  phase, acting, therefore, as plasticizers. Free volume effects may also exist.<sup>20</sup> It has been shown that blending of polymers generates additional free volume,<sup>21</sup> which can lower  $T_g$  by reducing the energy necessary for segmental motion. If one considers the additional possibility of some interactions between components and/or phases, it seems illusive to get information about phase compositions from  $T_{m\beta}$  using standard equations predicting the  $T_g$  of a blend from  $T_g$ s of components.  $T_{m\beta}$  is once again independent upon the PEI concentration and the cure schedule. This means that neither  $T_{m\alpha}$  nor  $T_{m\beta}$  can give information about the volume fraction or the shape of the phases.

On the other hand, more information may be obtained by regarding the heights of loss peaks and, more particularly, the ratio of these heights. Indeed, it appears to be very sensitive not only to the volume fraction but also to the shape of final morphologies through the choice of  $T_i$ , the cure temperature. The lowest values are then obtained for the 10P systems for which phase separation leads to the formation of  $\beta$  particles dispersed in a continuous  $\alpha$  phase (before phase inversion). The 20P system precured at 80°C, for which a

complete inverted structure was observed, presents the highest value of ( $h_\beta/h_\alpha$ ). The same system precured at higher temperatures, associated with the formation of bicontinuous structures, gives slightly lower values. The ratio ( $h_\beta/h_\alpha$ ) may consequently be an appropriate parameter to predict at least qualitatively the kind of morphology generated and to know if the structure is inverted or not. Note that, even if the values of the 10P blends remained very close, the highest value was obtained for  $T_i = 80^\circ\text{C}$ , i.e., when the connectivity of the  $\beta$  phase is the most important.

### Mechanical Properties

The mechanical properties such as Young's modulus,  $E$ , the Poisson's ratio,  $\nu$ , the critical stress intensity factor  $K_{Ic}$ , the critical strain energy release rate,  $G_{Ic}$ , and the upper yield stress,  $\sigma_y$  are reported in Table V. The kind of morphology obtained for each system is also indicated.

Because both  $E$  and  $\nu$  of the neat resin and pure PEI are relatively close, only slight changes could be expected for the blends. Therefore, when the continuous phase is the epoxy-rich phase, the modulus of blends is almost the modulus of the neat resin. A slight increase towards values closer to the PEI modulus is observed when bicontinuous and inverted structures are generated.

The fracture toughness,  $K_{Ic}$  is plotted Figure 7 as a function of the modifier concentration at the different precure temperatures studied. Whatever  $T_i$ , i.e. the shape of the dispersed  $\beta$  particles,  $K_{Ic}$  of the 10P blends remained almost unchanged and was not much higher than that of the neat

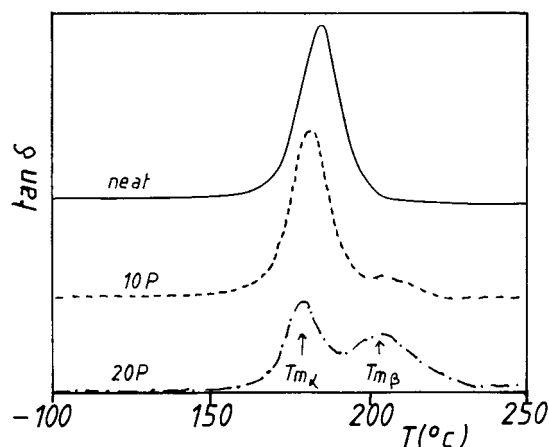


**Figure 6** Dynamic mechanical spectra: loss factor,  $\tan \delta$  vs. temperature for (—) neat epoxy matrix, (-----) 10P,  $T_i = 80^\circ\text{C}$ , (-·-·-) 20P,  $T_i = 80^\circ\text{C}$ .

**Table IV** Temperatures ( $T_{m\alpha}$ ,  $T_{m\beta}$ ), Heights ( $h_\alpha$ ,  $h_\beta$ ) and Ratio of Heights ( $\frac{h_\beta}{h_\alpha}$ ) for High Temperature Maxima Loss Peaks Depending on the System

System		Morphology	$T_{m\alpha}$ (°C)	$h_\alpha$	$T_{m\beta}$ (°C)	$h_\beta$	$\frac{h_\beta}{h_\alpha}$
Neat Matrix			184	0.92			
10P	$T_i = 80^\circ\text{C}$	particulate	180	0.77	204	0.14	0.18
10P	$T_i = 135^\circ\text{C}$	particulate	180	0.88	204	0.13	0.15
10P	$T_i = 160^\circ\text{C}$	particulate	181	0.85	205	0.13	0.15
20P	$T_i = 80^\circ\text{C}$	inverted	181	0.45	201	0.35	0.78
20P	$T_i = 135^\circ\text{C}$	bicontinuous	179	0.48	204	0.31	0.65
20P	$T_i = 160^\circ\text{C}$	bicontinuous	184	0.53	203	0.35	0.66
PEI				/	225	2.8	

epoxy matrix. Alternatively, the relative toughness improvement ( $\Delta K_{Ic}/K_{Ic0}$ ) can reach 85% for the 20P blend when precured at  $160^\circ\text{C}$ . For this modifier concentration,  $T_i$  has a stronger influence on fracture toughness because it has a stronger effect on final morphologies. For the same amount of additive, bicontinuous structures ( $T_i = 135^\circ\text{C}$ ,  $160^\circ\text{C}$ ) lead to more important toughness enhancement than inverted structures ( $T_i = 80^\circ\text{C}$ ). This shows the great influence of microstructures on subsequent mechanical properties. These results follow the trends apparent in the literature, i.e., the fracture toughness in such blends is significantly improved only when bicontinuous or phase-inverted structures are produced.<sup>22–24</sup>

The only published results defying this trend surprisingly concern tetrafunctional epoxy resins modified by the same PEI for which spectacular toughness improvements were reported before phase inversion.<sup>25,26</sup> Before discussing fracture/

toughening mechanisms, let us examine closer the load-displacement curves obtained from tests to determine  $K_{Ic}$ . Figure 8(a)–(c) shows three load-displacement curves corresponding respectively to the neat resin, 10P, and 20P blends precured at  $T_i = 160^\circ\text{C}$  for the same size of notches. It can be seen that the load does not fall to zero after having reached  $F_c$ , clearly exhibiting a semi-controlled crack propagation. Each curve can be divided into two parts: a first part associated to  $U_e$ , the stored elastic energy, and a second part associated to  $U_a$ , the additional energy required to the whole propagation of the crack. The determination of  $K_{Ic}$  only considers the load  $F_c$  leading to the initiation of the critical crack and does not take into account the propagation stage. The values  $(U_a/U_t) = (U_a/U_e + U_a)$  are given in Table VI as a function of PEI content. It appears that  $(U_a/U_t)$  increases with the modifier concentration. This means that even if no significant fracture toughness improvement is measured for 10P

**Table V** Kind of Morphology; Young's Modulus,  $E$ ; Poisson's Ratio,  $\nu$ ; Critical Stress Intensity Factor,  $K_{Ic}$ ; Critical Strain Energy Release Rate,  $G_{Ic}$ ; Upper Yield Stress,  $\sigma_y$  Depending on the System and Measured at  $25^\circ\text{C}$ 

System		Morphology	$E$ (GPa)	$\nu$	$K_{Ic}$ ( $\text{MPa} \cdot \text{m}^{1/2}$ )	$G_{Ic}$ ( $\text{J} \cdot \text{m}^{-2}$ )	$\sigma_y$ (MPa)
Neat Matrix			2.75	0.38	0.6	112	110
10P	$T_i = 80^\circ\text{C}$	particulate	2.77	0.37	0.69	148	110
10P	$T_i = 135^\circ\text{C}$	particulate	2.73	0.37	0.66	138	116
10P	$T_i = 160^\circ\text{C}$	particulate	2.80	0.37	0.64	126	118
20P	$T_i = 80^\circ\text{C}$	inverted	2.89	0.4	0.87	220	116
20P	$T_i = 135^\circ\text{C}$	bicontinuous	3.12	0.39	0.97	256	115
20P	$T_i = 160^\circ\text{C}$	bicontinuous	2.91	0.38	1.11	362	115
PEI			3.32	0.37	3.6 <sup>a</sup>	3400 <sup>a</sup>	/

<sup>a</sup> Values from ref. 4.



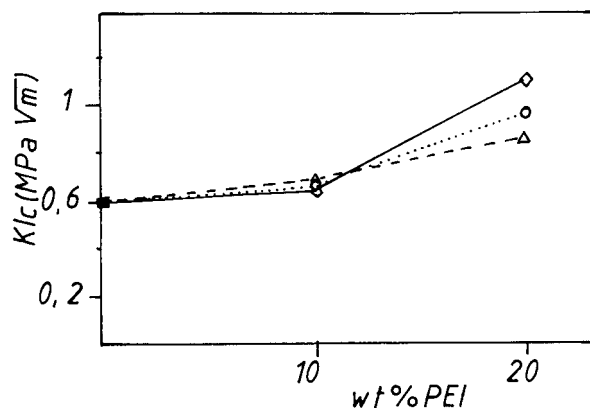


**Figure 7** Fracture toughness,  $K_{Ic}$  of final materials as a function of the modifier concentration, depending on the precure temperature ( $\triangle$ )  $T_i = 80^\circ\text{C}$ , ( $\circ$ )  $T_i = 135^\circ\text{C}$ , ( $\diamond$ )  $T_i = 160^\circ\text{C}$ , ( $\blacksquare$ ) neat.

blends, the PEI-rich particles nevertheless constitute obstacles to the propagation of the crack and/or contribute to the crack blunting effect. Charpy tests with unnotched specimens were then performed to highlight this toughness improvement, which does not appear from  $K_{Ic}$  measurements. Indeed, the surface resilience,  $R_S$  is a global measurement which takes into account not only the initiation of the crack resulting from the growth of intrinsic defects but also its propagation. The values of  $R_S$  obtained for samples precured at  $T_i = 160^\circ\text{C}$  are also reported in Table VI.  $R_S$  actually increases with 10 wt % of PEI and follows the same trend as  $(U_a/U_i)$ . We can then conclude that in our case rigid non functionalized thermoplastic particles have a small effect on  $K_{Ic}$  before phase inversion but act in the propagation step contributing to the strengthening of the material. However, some improvements have been found in the literature.<sup>6</sup>

SEM micrographs presenting the fracture surfaces of 10P and 20P samples are shown in Figure 9(a)–(f). For the 10P blends, the different shapes of  $\beta$  particles observed by TEM depending on the precure temperature are easily recognizable. The presence of voids corresponding to some  $\beta$  particles extracted clearly shows that brittle failure of the interface occurred without yielding

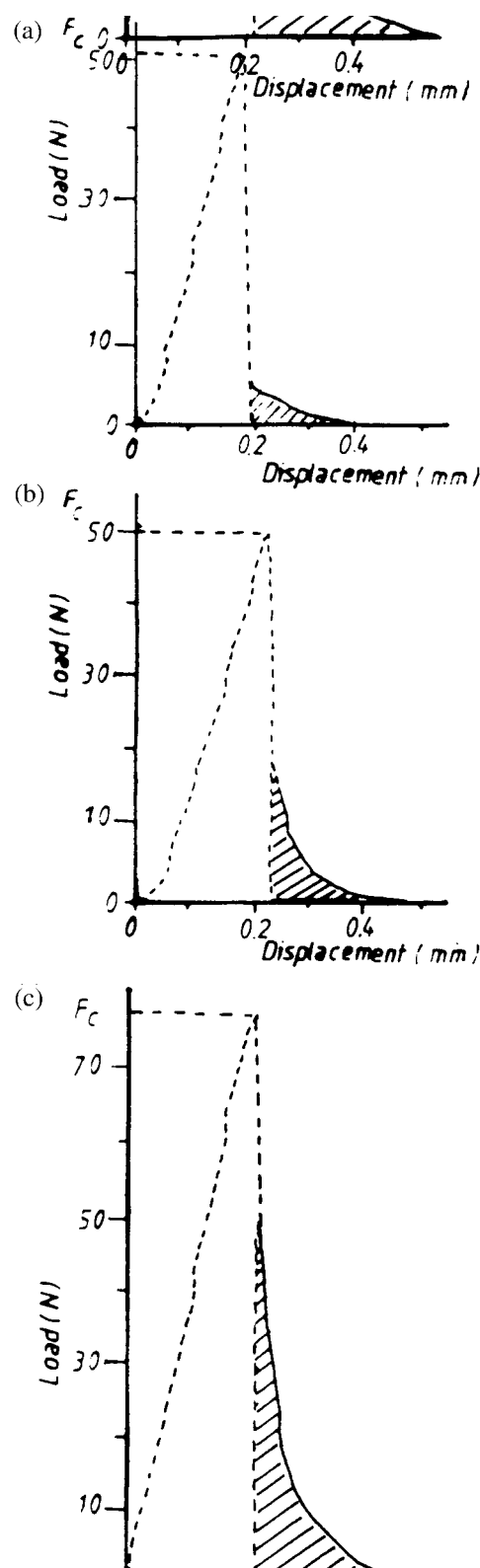


**Figure 8** Load–displacement curves got during three-point bending tests for (a) neat resin, (b) 10P  $T_i = 160^\circ\text{C}$ , (c) 20P  $T_i = 160^\circ\text{C}$  (same size of notches).  $F_c$  denotes the critical load, ( $\square$ ):  $U_e$ , the stored elastic energy, and ( $\text{hatched}$ ):  $U_a$ , the additional energy required to the crack propagation.

**Table VI**  $\frac{U_a}{U_t}$  and Surface Resilience,  $R_S$  as a Function of the Modifier Concentration for the Same Precure Temperature  $T_i = 160^\circ\text{C}$

System	$\frac{U_a}{U_t}$ (%)	$R_S$ ( $\text{kJ} \cdot \text{m}^{-2}$ )
neat	10.0	13.0
10P	20.8	17.0
20P	29.6	20.5

of rigid thermoplastic particles. The weak toughness improvement measured for the 10P blends is then probably due to a lack of interfacial adhesion, the PEI being nonfunctionalized. Obviously, the only observation of fracture surfaces is not sufficient to attribute the failure to any particular mechanism. But on the basis of more comprehensive works in this field,<sup>5,6,27,28</sup> an explanation of the failure process may be proposed. Inherently, differences in linear coefficients of thermal expansion creates thermal stresses at the matrix–inclusion interface. The external load added to pre-existing internal stresses then creates stress concentrations at the interface, resulting in the formation of interfacial microcracks. Pearson and Yee<sup>5</sup> assumed that the microcracking could be applicable to highly crosslinked epoxies because this mechanism does not require the shear deformation of the matrix. Because the interfacial adhesion is very weak, no drawing of particles can compensate for these dramatic stress concentrations and the microcracks induce the failure of inclusions more or less in the crack tip planes and, then, the macroscopic failure of the sample. The branching of the crack induced by this mechanism may explain the much disturbed relief of the surface compared to unmodified samples. Furthermore, the evidence of crack-pinning is shown by the presence of tails behind the particles (see micrograph 9b). In this mechanism, the rigid PEI-rich particles behave as impenetrable objects that cause the crack to bow out, which consumes extra energy. The occurrence of crack-pinning may explain the previously discussed increase of  $U_a$  with PEI content. Note that no voiding or cavitation is exhibited on fracture surfaces as well as no stress whitening.

For the 20P blends, micrographs 9–f show that the PEI-rich phase was strongly plastically drawn around undamaged epoxy domains. Once again, the interfacial adhesion appears to be poor, but a weak interface is probably helpful here to allow

this plastic deformation of the PEI-rich phase. The remaining question is why bicontinuous structures ( $T_i = 135^\circ\text{C}$ ,  $160^\circ\text{C}$ ) give higher toughness than an inverted structure ( $T_i = 80^\circ\text{C}$ ). It can be seen on micrograph 9d that no large debonding around epoxy-rich domains occurred. The high degree of interaction between phases in bicontinuous morphologies may facilitate a more uniform stress distribution in the material under load and thereby avoid premature failure by localized stress concentrations. The thickness of the  $\beta$  phase also increases with precure temperature (see TEM micrographs).

If we come back to the  $\sigma_y$  results, it is surprising to note that the increase of  $R_S$  with PEI content comes with an increase of  $\sigma_y$ . The opposite evolution is generally expected if the yielding phenomena is dominant.<sup>6,22</sup> To try to interpret our results, the strain recoveries of neat and modified systems were compared. Indeed, when a polymer is deformed in the glassy state, three components of its deformation are distinguished:<sup>29–31</sup> elastic, anelastic, and plastic deformation. The elastic strain,  $\epsilon_{el}$  recovers instantaneously, the anelastic one,  $\epsilon_{an}$  recovers over a large range of time, and the plastic one,  $\epsilon_{pl}$  is permanent. The value of  $\epsilon_{an}$  depends on the temperature test,  $T_{def}$ , diminishing as  $T_{def}$  increases. It is expected to become negligible when  $T_{def} > T_g$ .<sup>30</sup> On the other hand,  $\epsilon_{pl}$  is always present whatever  $T_{def}$ . It always recovers in the  $T_g$  zone during a heating of the sample. To determine these three components, samples were compressed until a deformation  $\epsilon_t = 18\%$  at a crosshead speed of  $0.5 \text{ mm} \cdot \text{min}^{-1}$ . The load was then quickly suppressed ( $30 \text{ mm} \cdot \text{min}^{-1}$ ). The remaining deformation after a recovery time of 30 min was measured and considered as the plastic deformation,  $\epsilon_{pl}$ . The values of  $\epsilon_{pl}$ ,  $\epsilon_{el}$ , and  $\epsilon_{an}$  measured for the different systems at room temperature in uniaxial compression are reported in Table VII.

Then it is apparent that (a) the main part of the total deformation is recovered at room temperature; (b) whatever the system, the anelastic contribution remains preponderant; (c) the anelastic part decreases with the modifier concentration; (d) the plastic part increases with modifier concentration; (e)  $\epsilon_{el}$ ,  $\epsilon_{an}$ , and  $\epsilon_{pl}$  seem independent of the cure conditions. This means in particular that the presence of 10 wt % PEI favors the plastic deformation of the matrix. The same conclusion can be drawn for the systems with 20 wt % PEI. This cannot be seen using the conventional  $\sigma_y$  value, the maximum of the strain–stress curve,

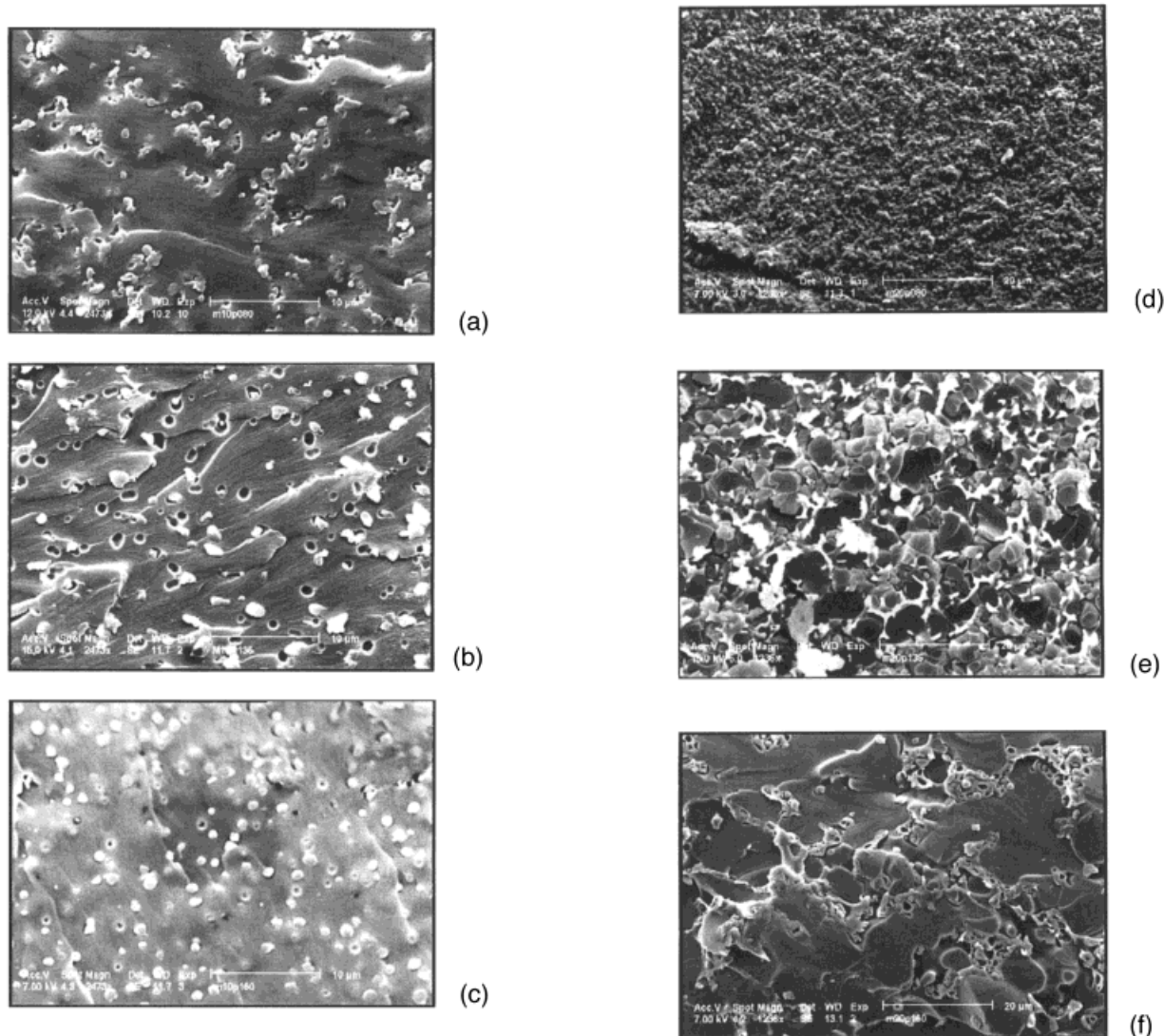


**Figure 9** Fracture surfaces observed by SEM of the 10P bends (a)  $T_i = 80^\circ\text{C}$ , (b)  $T_i = 135^\circ\text{C}$ , (c)  $T_i = 160^\circ\text{C}$ , and of the 20P blends (d)  $T_i = 80^\circ\text{C}$ , (e)  $T_i = 135^\circ\text{C}$ , (f)  $T_i = 160^\circ\text{C}$ .

because the strain is mainly anelastic at this point. These results are now consistent with  $R_S$  improvement. A description of the deformation

processes was proposed by Perez et al.<sup>32,33</sup> At a macroscopic level, the anelastic deformation is associated to localized strained zones called shear

**Table VII** Upper Yield Stress,  $\sigma_y$ , in Uniaxial Compression at  $25^\circ\text{C}$ ; Elastic Strain Part,  $\epsilon_{el}$ ; Anelastic Strain Part,  $\epsilon_{an}$  and Plastic Strain Part,  $\epsilon_{pl}$  for  $\epsilon_t = \epsilon_{el} + \epsilon_{an} + \epsilon_{pl} = 18\%$  Depending on the System

System		$\sigma_y$ (MPa)	$\epsilon_{el}$ (%)	$\epsilon_{an}$ (%)	$\epsilon_{30'} \approx \epsilon_{pl}$ (%)
Neat matrix		110	4.3	10.9	2.7
10P	$T_i = 80^\circ\text{C}$	110	3.7	8.9	5.4
10P	$T_i = 135^\circ\text{C}$	116	4.1	8.5	5.2
20P	$T_i = 80^\circ\text{C}$	116	3.9	7.2	6.8
20P	$T_i = 135^\circ\text{C}$	115	4.0	7.7	6.2

microdomains (SMD) in an undeformed matrix. These SMD correspond to an increase in potential energy. After unloading, most of these SMD fast recover at  $T_{\text{def}}$ . The plastic deformation results from SMD interaction and annihilation when they are numerous and large enough, and corresponds to a chain orientation, which creates a rubber-like entropic force. Chain orientation corresponds to new stable configurations and needs a very long time or a high thermal energy (temperature close to  $T_g$ ) to return to the initial configuration under the effect of the entropic force.

It can be now concluded that if microcracking and crack pinning are toughening mechanisms involved in these systems before phase inversion, the particle-induced shear yielding of the matrix is nevertheless present.

## CONCLUSION

The control of morphologies generated during a reaction-induced phase separation procedure is essential to control the mechanical properties of final materials. This requires effective control of cure kinetics and the phase separation process. Appropriate precuring and postcuring schedules must be selected on the basis of temperature-conversion-transformation diagrams.

The precure temperature has a strong effect on morphologies because it affects the viscosity of the system at the cloud point and the extent of the phase separation process. The ratio of the heights of the loss peaks corresponding to each phase appeared to be an appropriate parameter to predict qualitatively the kind of morphology generated and to know if the structure is inverted or not. Unfortunately, viscoelastic measurements could not give quantitative information on phase composition, which remains the main unknown in such systems.

The fracture toughness of blends was found to be significantly improved only when bicontinuous or inverted structures are generated. Before phase inversion, the thermoplastic-rich particles nevertheless constitute obstacles to crack propagation. This strengthening of the material was highlighted through impact resistance measurements. The occurrence of microcracking and crack-pinning in these materials before phase inversion was shown as well as the particle-induced shear yielding of the matrix. These results show such a nonfunctionalized additive leads to poor interfacial adhesion, and consequently, disap-

pointing mechanical properties. The synthesis and the use of functionalized thermoplastics to toughen brittle epoxy matrix is, as a result, under development. The introduction of appropriate copolymers as emulsifiers in blends may be an alternative route to increase the interfacial adhesion. Work in this field is in progress in our group.

The authors wish to thank the Centre de Microscopie Electronique Appliquée à la Biologie et à la Géologie (CMEABG), and especially Isabelle Bernard for preparing ultrathin sections, and the Direction Recherche Etudes et Techniques (DRET) for financial support.

## REFERENCES

1. H. J. Sue, E. I. Garcia-Meitin, D. M. Pickelman, and P. C. Yang, in *Rubber Toughened Plastics I*, C. K. Riew, Ed., Advances in Chemistry Series 233, American Chemical Society, Washington, DC, 1993, p. 405.
2. C. Girodet, E. Espuche, H. Sautereau, B. Chabert, R. Ganga, and E. Valot, *J. Mater. Sci.*, **31**, 2997 (1996).
3. L. Becu, H. Sautereau, A. Maazouz, J. F. Gérard, M. Pabon, and C. Pichot, *Polym. Adv. Technol.*, **6**, 316 (1995).
4. C. B. Bucknall and I. K. Partridge, *Polymer*, **24**, 639 (1983).
5. R. A. Pearson and A. F. Yee, *Polymer*, **34**, 3658 (1993).
6. R. A. Pearson, in *Rubber Toughened Plastics I*, C. K. Riew and A. J. Kinloch, Eds., Advances in Chemistry Series 233, American Chemical Society, Washington, DC, 1993, p. 405.
7. R. J. J. Williams, B. A. Rozenberg, and J. P. Pascault, *Adv. Polym. Sci.*, **128**, 95 (1997).
8. L. C. Chan, J. K. Gillham, A. J. Kinloch, and S. J. Shaw, in *Rubber-Modified Thermoset Resins*, C. K. Riew and J. K. Gillham, Eds., Advances in Chemistry Series 208, American Chemical Society, Washington, DC, 1994, p. 235.
9. D. Verchere, J. P. Pascault, H. Sautereau, S. M. Moschiar, C. C. Riccardi, and R. J. J. Williams, *J. Appl. Polym. Sci.*, **42**, 701 (1991).
10. L. T. Manzione, J. K. Gillham, and L. A. MacPherson, *J. Appl. Polym. Sci.*, **26**, 889 (1981).
11. A. Seris, J. P. Pascault, and Y. Camberlin, in *Polyimides and Other High-Temperature Polymers*, J. M. Abadi and B. Sillion, Eds., Elsevier Science Publishers, Amsterdam, 1991, p. 347.
12. E. Girard-Reydet, C. C. Riccardi, H. Sautereau, and J. P. Pascault, *Macromolecules*, **28**, 7599 (1995).
13. E. Girard-Reydet, C. C. Riccardi, H. Sautereau,

- and J. P. Pascault, *Macromolecules*, **28**, 7806 (1995).
14. C. C. Riccardi, J. Borrajo, R. J. J. Williams, E. Girard-Reydet, H. Sautereau, and J. P. Pascault, *J. Polym. Sci., Polym. Phys.*, **34**, 349 (1996).
  15. E. Girard-Reydet, J. P. Pascault, H. Sautereau, P. Navard, S. Keates, G. Thollet, and G. Vigier, *Polymer* (accepted).
  16. J. G. Williams and M. J. Cawood, *Polym. Test.*, **9**, 15 (1990).
  17. G. Merle, Y. S. O. C. Pillot, and H. Sautereau, *Polym. Test.*, **5**, 37 (1985).
  18. N. Clarke, T. C. B. McLeish, and S. D. Jenkins, *Macromolecules*, **28**, 4650 (1995).
  19. C. B. Bucknall, C. M. Gomez, and I. Quintard, *Polymer*, **35**, 353 (1994).
  20. M. Akay and J. F. Cracknell, *J. Appl. Polym. Sci.*, **52**, 663 (1994).
  21. M. Akay and S. N. Rollins, *Polymer*, **34**, 1865 (1993).
  22. A. J. MacKinnon, S. D. Jenkins, P. T. McGrail, and R. A. Pethrick, *Macromolecules*, **25**, 3492 (1992).
  23. A. J. Kinloch, M. L. Yuen, and S. D. Jenkins, *J. Mater. Sci.*, **29**, 3781 (1994).
  24. R. W. Venderbosch, H. E. H. Meijer, and P. J. Lemstra, *Polymer*, **35**, 4349 (1994).
  25. C. B. Bucknall and A. H. Gilbert, *Polymer*, **30**, 213 (1989).
  26. J. Jang and S. Shin, *Polymer*, **36**, 1199 (1995).
  27. R. S. Raghava, *J. Polym. Sci., Polym. Phys.*, **25**, 1017 (1987).
  28. R. S. Raghava, *J. Polym. Sci., Polym. Phys.*, **26**, 65 (1988).
  29. R. Quinson, J. Perez, M. Rink, and A. Pavan, *J. Mater. Sci.*, to appear.
  30. E. Oleynick, *Prog. Colloid Polym. Sci.*, **80**, 140 (1989).
  31. E. Oleynick, in *High Performance Polymers*, X. Baer, Ed., Munich, 1990, p. 79.
  32. J. Y. Cavaillé, J. Perez, and G. P. Johari, *Phys. Rev.*, **B39**, 2411 (1989).
  33. J. Perez, in *Physique et Mécanique des Polymères Amorphes*, Lavoisier, Paris, 1992.